Planetary and Space Science 117 (2015) 329–344

Contents lists available at ScienceDirect

Planetary and Space Science

journal homepage: www.elsevier.com/locate/pss

The Ma_Miss instrument performance, II: Band parameters of rocks powders spectra by Martian VNIR spectrometer

Simone De Angelis [a,*], Maria Cristina De Sanctis [a], Eleonora Ammannito [a,b], Cristian Carli [a], Tatiana Di Iorio [c], Francesca Altieri [a]

[a] Institute for Space Astrophysics and Planetology, INAF – IAPS, via Fosso del Cavaliere, 100, 00133 Rome, Italy
[b] Department of Earth, Planetary and Space Sciences – UCLA, Los Angeles, CA, USA
[c] ENEA, UTMEA-TER, Rome, Italy

ARTICLE INFO

Article history:
Received 3 April 2015
Received in revised form
7 July 2015
Accepted 8 July 2015
Available online 29 July 2015

Keywords:
ExoMars
Ma_Miss
VNIR spectroscopy
Mars

ABSTRACT

The Ma_Miss instrument (Mars Multispectral Imager for Subsurface Studies, Coradini et al. (2001)) is a Visible and Near Infrared miniaturized spectrometer that will observe the Martian subsurface in the 0.4–2.2 μm spectral range. The instrument will be entirely hosted within the Drill of the ExoMars-2018 Pasteur Rover: it will allow analyzing the borehole wall excavated by the Drill, at different depths, down to 2 m. The aim will be to investigate and characterize the mineralogy and stratigraphy of the shallow Martian subsurface.

A series of spectroscopic measurements have been performed in order to characterize the spectral performances of the laboratory model of the instrument (breadboard). A set of six samples have been analyzed. Each sample (four volcanic rocks, a micritic limestone and a calcite) has been reduced in particulate form, ground, sieved and divided into nine different grain sizes in the range $d < 0.02 \div 0.8$ mm. Spectroscopic measurements have been performed on all samples using two distinct experimental setup: (a) the Ma_Miss breadboard, and (b) the Spectro-Goniometer setup, both in use in the laboratory at INAF – IAPS.

In a previous paper spectral parameters such as the continuum slope and the reflectance level of the spectra have been discussed (De Angelis et al., 2014).

In this work we focus our discussion on absorption band parameters (position, depth, area, band slope and asymmetry). We analyzed/investigated the absorption features at 1 μm for the volcanic samples and at 1.4, 1.9 and 2.2 μm for the two carbonate samples. Band parameters have been retrieved from spectra measured with both experimental setup and then compared.

The comparison shows that band parameters are mutually consistent: band centers (for carbonate samples) are similar within few percent, and band depth and area values (for carbonates) show consistent trends vs. grain size (decreasing towards coarser grains) for most of samples.

1. Introduction

The ESA ExoMars Project will study the Martian environment by means of an Orbiter (2016 mission) and a Rover (2018 mission) (Vago et al., 2013). The 2016-mission will bring a Trace Gas Orbiter (TGO), with the aim of studying trace gases (such as, for example, methane) and the atmospheric environment, and an Entry, Descent and Landing Demonstrator Module (EDM) hosting instruments for the investigation of the atmosphere and environment at ground level. The 2018-mission foresees a Rover (Pasteur) carrying on board several instruments for the analysis of mineralogy, geology and geochemistry of the surface and subsurface. The Rover also has a drilling system, which will be able to perforate the Martian surface at different depths, down to a maximum of 2 m. The Drill hosts the Ma_Miss (Mars Multispectral Imager for Subsurface Studies) instrument, a miniaturized spectrometer devoted to study the Martian subsurface. Ma_Miss will acquire spectra and characterize the mineralogy and the stratigraphy of the shallow subsurface down to 2 m. The Drill is also designed to collect samples at various depths and to provide them to a suite of instruments on board the Rover vehicle. This suite of instruments will perform chemical, physical and spectral analyses on the collected samples, thus working exactly like an analytical laboratory.

In this work we focus on the characterization of spectral performances of the breadboard of Ma_Miss instrument. Reflectance spectra have been acquired with two different experimental

* Corresponding author. Tel: +39 06 49934083.
E-mail address: simone.deangelis@iaps.inaf.it (S. De Angelis).

http://dx.doi.org/10.1016/j.pss.2015.07.002
0032-0633/

setups (Ma_Miss breadboard and Spectro-Goniometer) on six Martian analog samples in powder form, each sieved in nine different grain sizes. Different spectral parameters have been determined and thus compared. In particular here band parameters, such as position, width, depth, area and asymmetry are taken into account, while in a previous work (De Angelis et al., 2014) the continuum slope and the reflectance level were studied. Here we report only a brief description of the instrument and laboratory setup; the details can be found in De Angelis et al. (2014).

1.1. The surface and subsurface of Mars

Volcanic rocks are the main and more widespread constituents of the surface of Mars (see for example Mustard et al. (1997), Bandfield et al. (2000), Bandfield (2002), McSween et al. (2009), Ehlmann and Edwards (2014)). Primary minerals that characterize the crust are olivine, clinopyroxenes, orthopyroxenes, plagioclases, high-silica phases (zeolites, silicate glasses) (Ehlmann and Edwards, 2014).

The morphological dichotomy of the Martian surface is also reflected into mineralogy: the Southern Highlands are dominated by clinopyroxenes and plagioclases; in the Northern Plains the pyroxenes are not widespread, and high-silica phases are the dominant component (Ehlmann and Edwards, 2014). Mafic/ultramafic rocks are the main components of the older crust: olivine-rich materials are exposed in many craters walls and ejecta. Olivine varies in the range Fo_{40}–Fo_{90}, and almost globally it appears on the rims of largest impact basins.

More recently, the lithologies that were initially associated to andesitic compositions (Bandfield et al., 2000; Bandfield, 2002), have been attributed to weathering products of basalts (McSween et al., 2009); more evolved volcanic rocks (i.e. with high Si content, >65 wt%) are not very diffuse on the surface of Mars, although recently felsic rocks have been identified at Syrtis Major and Noachis Terra (Wray et al., 2013). Christensen et al. (2005) also report the observation of dacites (high-Si lavas) in the Syrtis Major caldera.

Moreover, several evidences indicate that the ancient climate of Mars was hotter and wetter than today.

One of the main evidences for the different climate condition are the presence of fluvial systems on the planet's surface (e.g., Bibring, 2005). Some authors indicate as particular geomorphologic features (e.g., shorelines) can be interpreted as due to an Hesperian (3–3.7 Gyr) ocean in the Northern Hemisphere (Carr and Head III, 2003; Dohm et al., 2009). Nevertheless other evidencies indicate that were present valley networks (Noachian period, 3.7–4.6 Gyr), large outflow channels (Hesperian) (Carr and Head III, 2010), as well as lacustrine environments (such as Shalbatana paleolake, Di Achille et al., 2013; Squyres et al., 2004). Observations from Mars Science Laboratory (mission description in Grotzinger et al. (2012)) have shown the signs of ancient fluvial activity. Outcrops of cemented rounded pebbles (with clast sizes of few mm in diameter) at the Gale Crater (Williams et al., 2013) are explained with the action of ancient water flows, that has caused movement and abrasion of clasts. Silt and sandstone have been observed at Yellowknife Bay by MAHLI camera (Edgett et al., 2013); depositional structures and cross-stratified sedimentary rocks observed at Shaler and Rocknest (Gupta et al., 2013) are explained with ancient fluvial activity.

From a spectroscopical point of view the different climatic condition are indicated by the presence of hydrate materials, like water-bearing phyllosilicates, such as nontronite, chamosite and montmorillonite, that have been detected by OMEGA data (e.g. Poulet et al., 2005). Those mineral phases could be originated by aqueous alteration of mafic and sialic minerals, and so an indication of the existence of liquid water environments early on Mars. Phyllosilicate outcrops and clay-rich layers show in some cases very large extensions (Poulet et al., 2005) and this is consistent with very long periods (geological timescales) in which igneous rocks have been in contact with liquid water. Many types of aqueous minerals have been detected, subdivided into different classes on the basis of spectral absorptions, of geographic occurrence and morphologic features (see review by Murchie et al. (2009) and Ehlmann and Edwards (2014)).

Detections of hydrated sulfate minerals in layered terrains in Valles Marineris, Margaritifer Terra and Terra Meridiani (e.g. Gendrin et al., 2005; Murchie et al., 2009; Ehlmann and Edwards, 2014) are consistent with kieserite, gypsum and epsomite. The presence of hydrated sulfates in different layers and depths of Valles Marineris can be explained with the evaporation of extensive water bodies (lakes or lagunas), although sulfates can also form in hydrothermal environments. Hydrated Ca-sulfates (gypsum) have been observed recently in rock veins at Gale Crater (MSL Mastcam observations, Rice et al. (2013)), while non-hydrated Ca-sulfates (anhydrite) have been detected at Yellowknife Bay (MSL ChemCam data, Nachon et al. (2013)).

For what concerns the carbonates, Mg-rich species of carbonates (huntite and magnesite) have been suggested by TES data (Palomba et al., 2009). Magnesite-plagioclases mixtures have been invoked to explain particular spectral signatures in Martian dust detected by TES (Niles et al., 2013). Spectral features attributed to Mg-rich carbonates (in mixtures with olivine and nontronite) have also been detected in CRISM data (in Noachian terrains, Nili Fossae; Ehlmann et al., 2008). Ca-carbonates (calcite, aragonite) have been detected using calorimetry techniques (Boynton et al., 2009) at the Phoenix landing site (Heimdall Crater). The recent detection of Ca- and/or Fe-carbonates at Huygens Crater (CRISM data, Wray et al. (2011)) is based on the observation of the carbonate absorption bands in the 2.3–2.5 μm region.

Large amounts of water could be, at the present day, stored in the Martian subsurface in form of permafrost, as suggested by several observations. Geomorphological features such as polygonal terrains, mass-movement phenomena, thermokarst or layering of crater ejecta (Carr and Schaber, 1977; Baker, 2001; Bibring, 2005; McEwen et al., 2013) could be related to the presence of subsurface ice. Water ice in the upper few meters of the Martian subsurface is also inferred by measurements of depth dependence of hydrogen abundances, thanks to the detection of neutrons and gamma rays (Boynton et al., 2002).

1.2. Ma_Miss instrument

Ma_Miss (Mars Multispectral Imager for Subsurface Studies) (Coradini et al., 2001) is a miniaturized Visible and Near Infrared spectrometer, designed to be completely integrated within the Drill of the Rover. The Ma_Miss spectral range is 0.4–2.2 μm, with a spectral sampling of about 20 nm and a spatial resolution of 120 μm. The radiation source for the whole spectral range is a 5 W lamp, integrated within the Drill Tip. A bundle of optical fibers conveys the light from the lamp to the Optical Head, which consists of several mirrors and is used to focus the light on the sample. A hard and transparent Sapphire Window, embedded in the Tip, protects the Optical Head, because the instrument must observe the vertical borehole wall excavated by the Drill. The light is focused on the target within a 1-mm diameter spot, outside the Sapphire Window at a distance of less than 1-mm. The Optical Head recollects the scattered signal from the target, from a 0.12 mm-diameter spot. A series of optical fibers then carries the recollected signal to the Spectrometer, which is hosted within the Drill Box. The instrument can acquire spectra at different depths, down to a maximum of 2 m: a series of extension rods of 50 cm of

length, hosting inside optical fibers, can be mounted on the Drill Tip in order to reach different depths.

The Thermo-Electric Cooler (for detector cooling), a calibration target (for radiometric calibration) and the Proximity Electronics are hosted inside the Drill Box.

1.3. Ma_Miss Breadboard setup

The laboratory model of the instrument (*breadboard*, BB) is installed at INAF – IAPS, Rome. It consists of the main subsystems, except the spectrometer: the 5 W lamp, the Illumination Bundle, the Optical Head, the Sapphire Window, the Signal Link here constituted by two connected optical fibers. In this setup the breadboard is coupled with a commercial spectrometer, the FieldSpec Pro©, with spectral range 0.35–2.5 μm. The Ma_Miss BB Optical Head allows a spatial resolution of 0.12 mm. This setup is described in higher details in De Angelis et al. (2014).

1.4. Spectro-Goniometer setup

The Spectro-Goniometer (SPG) setup (Coradini et al., 2005) is operative at INAF – IAPS, Rome. The radiation source is an 84 W Quartz Halogen Tungsten lamp. A commercial spectrometer, the FieldSpec Pro©, is used. Both the spectrometer and the light source are coupled with a goniometer: in this way it is possible to vary the illumination (i) and the emission (e) angle at different values. In this work the angle values are set at 30° and 0° respectively. The spectral range is the same as in the previous setup, and the spatial resolution is about 6 mm in diameter.

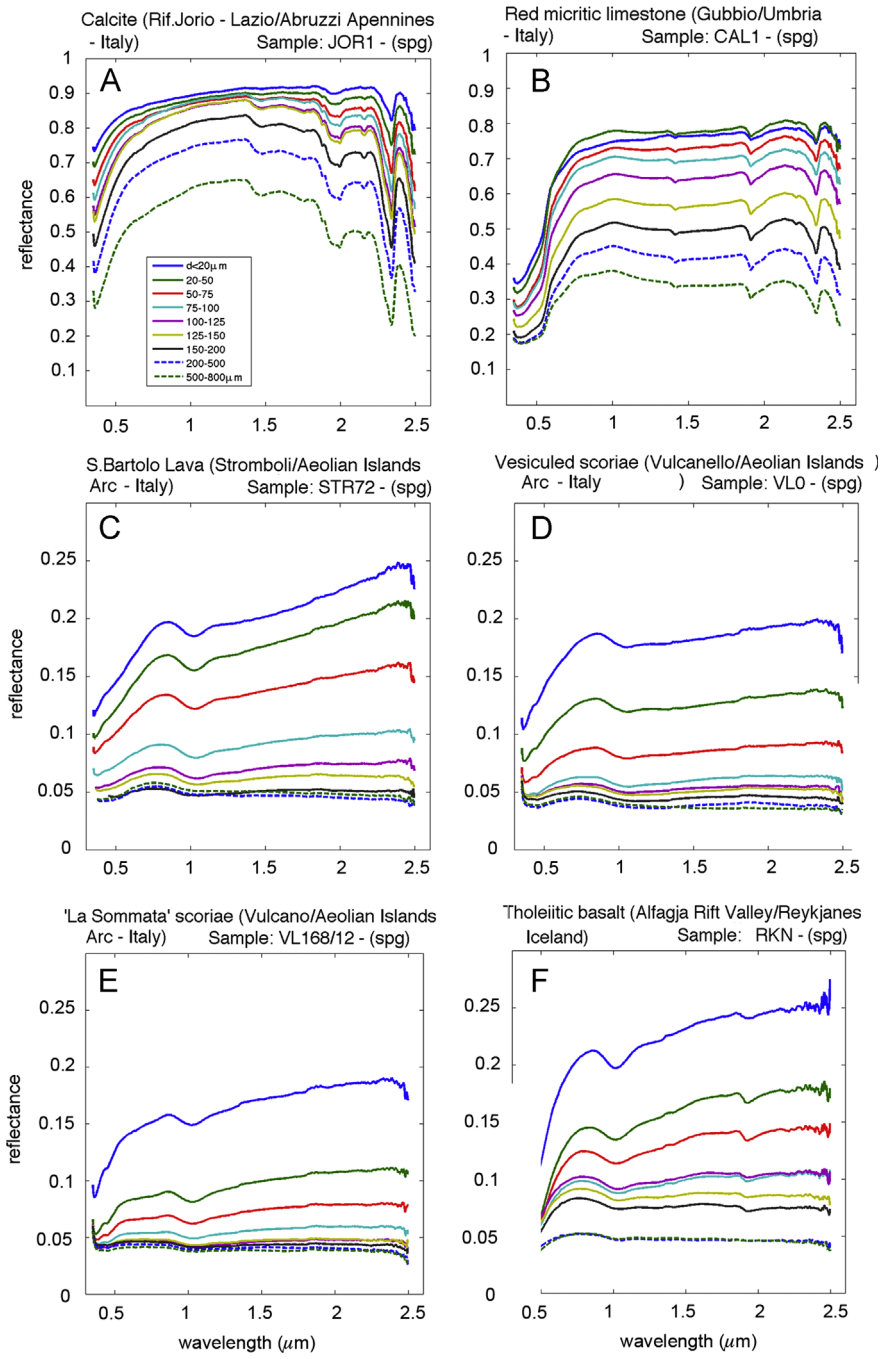

Fig. 1. Reflectance spectra acquired with Spectro-Goniometer setup.

2. Samples and measurements

Six samples in powder form have been analyzed with both instruments. The samples are a calcite (JOR1), a red micritic limestone (CAL1), a lava from Stromboli (STR72), two scoriae from Vulcano (VL168/12 and VL0) and a vesicular basalt from Iceland (RKN1) (see De Angelis et al. (2014) and references therein for samples' description). All samples have been previously grinded starting from rock fragments, and then sieved in nine different grain sizes in the range $d<0.02$–$d<0.8$ mm, where d is the grain diameter.

Reflectance spectra have been acquired for each sample, in each of the nine grain sizes, with both the setup. Labsphere© Spectralon reference targets have been used for radiometric calibration. A correction has been applied to take into account the Spectralon reflectance properties. In order to reduce grain size effects, due to the fact that Ma_Miss spatial spot is comparable with grain dimensions, Ma_Miss BB spectra have been acquired in 4 different positions on finer grains ($d<0.02$–0.1 mm), in 6 positions on intermediate grains ($d=0.1$–0.5 mm) and in 10 positions on coarser ones ($d=0.5$–0.8 mm), and then spatially averaged. Moreover, in order to increase the signal-to-noise ratio, 100 temporal averages have been computed for spectra in the VIS (0.35–1.0 μm) and NIR (1.0–1.8 μm) range, while 500 temporal averages have been computed in the IR (1.8–2.5 μm) spectral range. The spectra are showed in Fig. 1 (SPG), Fig. 2 (SPG, only volcanics, normalized at 0.8 μm) and Fig. 3 (Ma_Miss BB). The spectra acquired with Ma_Miss BB setup show two gaps in the data around 1 μm and 1.8 μm. This is due to the fact that at the juncture between the Vis–NIR and NIR–IR detectors, respectively, data are too noisy and so a number of points have been canceled.

3. Band analyses and results

Here we focused on the analysis of the absorption bands. The band at 1 μm has been considered for volcanic samples (RKN, STR72, VL0 and VL168/12) (the only occurring feature, except the H_2O band at 1.9 μm in RKN spectra). For the carbonate samples (JOR1 and CAL1), the bands at 1.4, 1.9 and 2.2 μm have been considered. The JOR1 sample also shows a feature at 1.75 μm, attributable to CO_3^{2-} (Gaffey, 1986), that is clearly visible in SPG spectra but is very faint in BB spectra. Additional bands occur in CAL1 spectra at 0.9 and 1.2 μm due to Fe^{3+} and Fe^{2+} (Burns, 1993); the absorption at 1.2 μm is not visible in BB spectra because points at the junction of VIS and NIR detectors have been cut.

Different types of parameters have been derived for the carbonate and volcanic samples:

Carbonates:
Band center
Band depth
Band area
Volcanics:
Band area (SPG spectra) and corrected band area (Ma_Miss BB)
1-μm band Short Wavelength slope (1-μm band θ_{SW})
1-μm band Long Wavelength slope (1-μm band θ_{LW})
1-μm band asymmetry parameter

Regarding the carbonate samples, band center, depth and area have been determined for each of the three considered features at 1.4, 1.9 and 2.2 μm.

In order to determine the band center (B_C), a straight line (in the wavenumber vs. log reflectance domain) has been tracked between the band wings λ_1 and λ_2, and then removed by division,

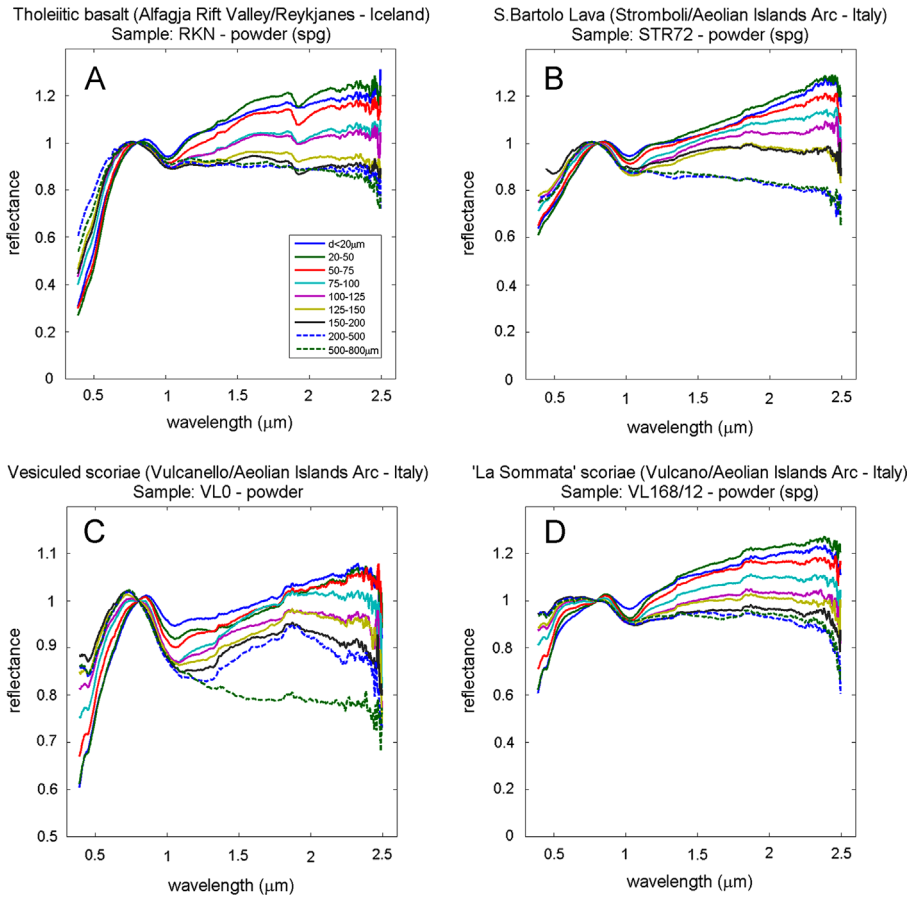

Fig. 2. Reflectance spectra acquired with Spectro-Goniometer setup. Volcanic samples spectra have been normalized at $\lambda=0.8$ μm, in order to highlight variations in spectral shape/slope.

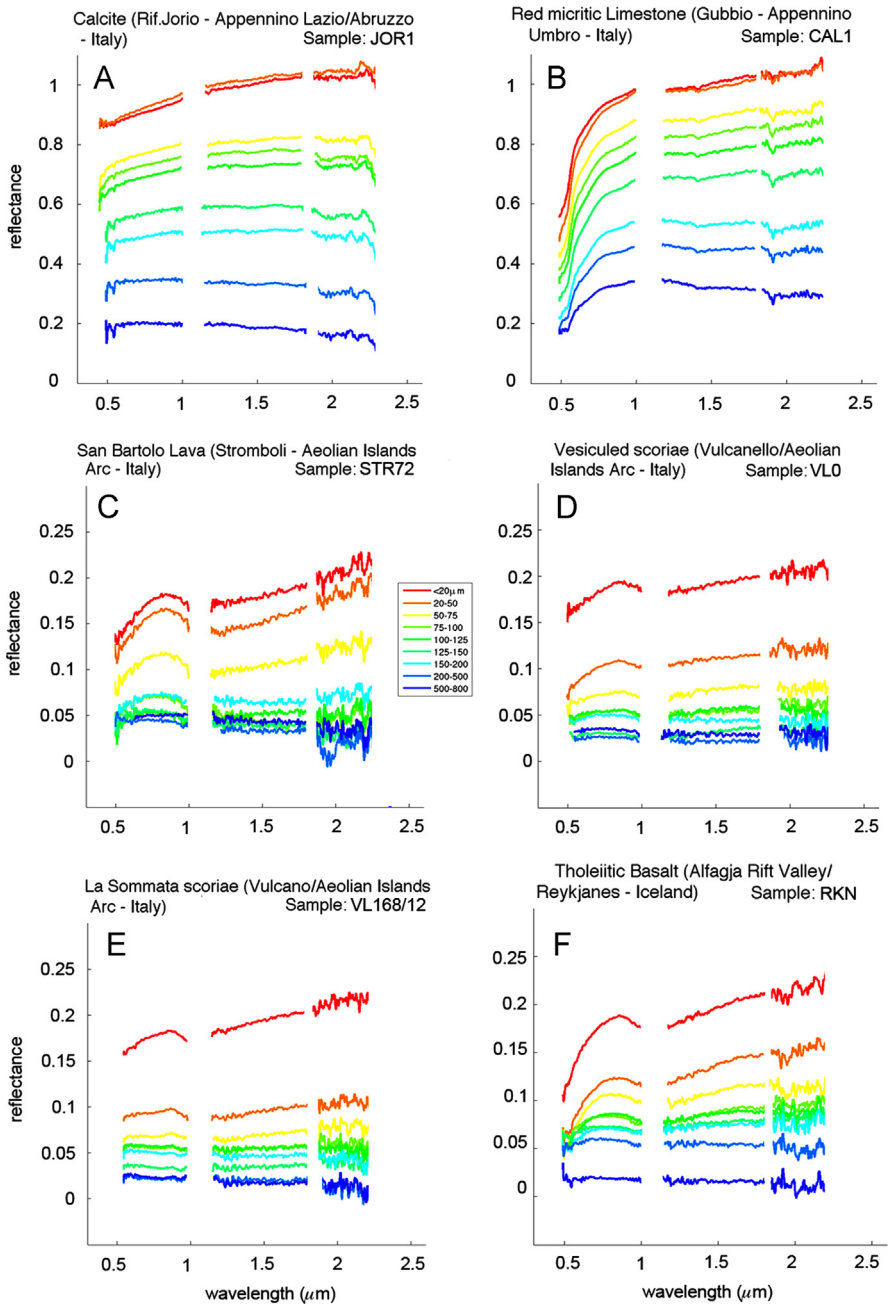

Fig. 3. Reflectance spectra acquired with Ma_Miss breadboard setup. The spectra acquired with Ma_Miss BB setup show two gaps in the data at around 1 μm and 1.8 μm, because data are too noisy at the juncture between the Fieldspec's detectors. See the text for more details.

for the continuum removal (Figs. 4 and 5). Subsequently a second order polynomial fit has been computed in the neighborhood of the center. The band position has been chosen as the vertex of the parabolic fit.

The band depth B_D has been determined according to Clark and Roush (1984) using the formula

$$B_D = \frac{R_C - R_B}{R_C}$$

where R_B is the reflectance at band center and R_C is the corresponding reflectance at the continuum.

The band area B_A has been obtained as the integral of the curve (continuum removed spectrum) between the two wings (Fig. 5A)

$$B_A = \int_{\lambda 1}^{\lambda 2} R(\lambda) d\lambda$$

where λ is the wavelength and R is the reflectance.

Concerning the spectra of volcanic samples, the centers and depths have not been determined for the band at 1 μm, because of the high noise in those spectral regions. It must be recalled that the noise is due to laboratory spectrometer associated with the BB that has 3 different detectors to cover the range 0.35–2.5 μm. The Ma_Miss instrument will have only one detector spanning the whole spectral range.

For these samples we computed: the sum of band areas on the left and the right size of the gap (*corrected band area*), the slope of the band on the Short and Long Wavelength side (angle θ_{SW} and

θ_{LW}), and the asymmetry parameter defined as ratio of the slopes of the visible and infrared side ($p=\theta_{SW}/\theta_{LW}$) (Fig. 5B).

The band area in this case is computed as

$$B_{AC} = \int_{\lambda 1}^{\lambda 2} R(\lambda)d\lambda + \int_{\lambda 3}^{\lambda 4} R(\lambda)d\lambda$$

The last three parameters (band slope in the Short/Long Wavelength side and asymmetry parameter) have been determined also for the spectra obtained with the SPG setup.

The computed parameters have been plotted as a function of the grain size for each sample for both instruments, and then compared (see the following sections and Figs. 7–16).

Statistic error bands have been determined for what concerns band slopes (SW and LW) and the asymmetry parameter. Details on calculations are reported in Appendix 1.

A fundamental source of error in the retrieving of band spectral parameters is given by the arbitrary choice of the continuum background. Generally a straight line is chosen as continuum. Nevertheless, in order to estimate this error, we computed the continuum in three different ways for one sample (RKN) and then determined two parameters (band area and depth at 1 μm) for both instruments (Fig. 6). The estimated errors are listed as an example in Tables 1 and 2.

3.1. Lava from Alfaja Rift Valley/Reykjanes – Iceland (RKN)

The spectra of this lava sample from Iceland are showed in Figs. 1F (SPG spectra) and 3F (Ma_Miss BB spectra). Spectra are characterized by the Crystal Field (CF) absorption feature at 1 μm (Fe^{2+}; Burns (1993)) and by the feature at 1.9 μm (H_2O; Clark et al. (1990), Clark (1999)); the water band is visible in BB spectra only in finer grains. Here we only considered the CF band. Band parameters have not been computed for 500–800 μm grain size interval.

Band area (Fig. 7A) values show a net decreasing trend with increasing grain size. Band area values from BB spectra are shifted downward of about 20%. Band areas computed from Ma_Miss spectra are systematically lower than areas retrieved from SPG data because of the gap at 1 μm.

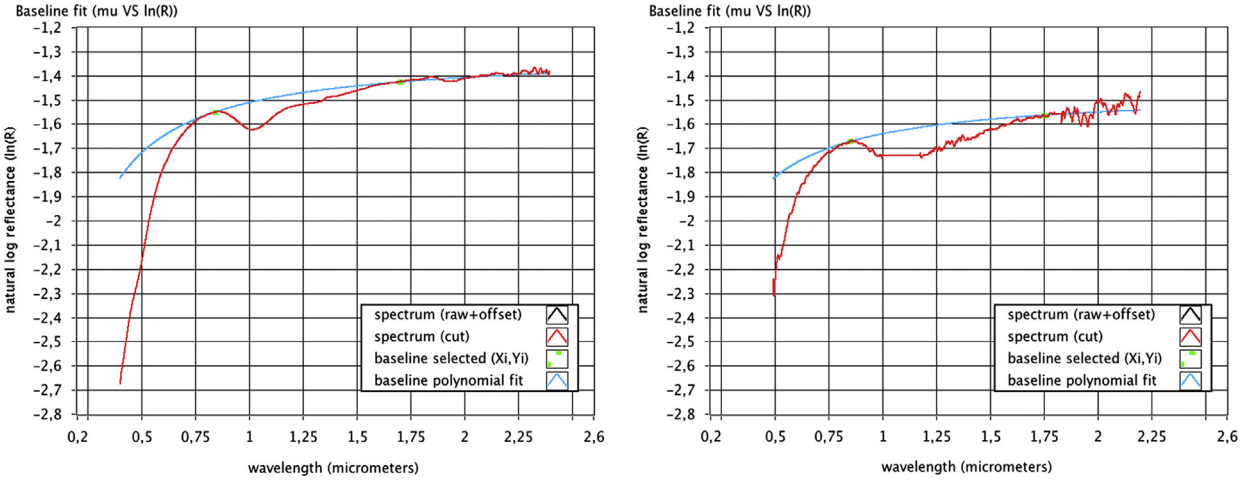

Fig. 4. Example of continuum background subtraction, for the sample RKN ($d<20$ μm; left: SPG. Right: Ma_Miss BB). Here the feature to analyze is the 1-μm band: the extremes (green squares) have been set at 0.85 and 1.7 μm. The continuum (blue curve) is a straight line in the ln R vs. wavenumber space, while it is a logarithm in the ln R vs. wavelength space. (For interpretation of the references to color in this figure legend, the reader is referred to the web version of this article.)

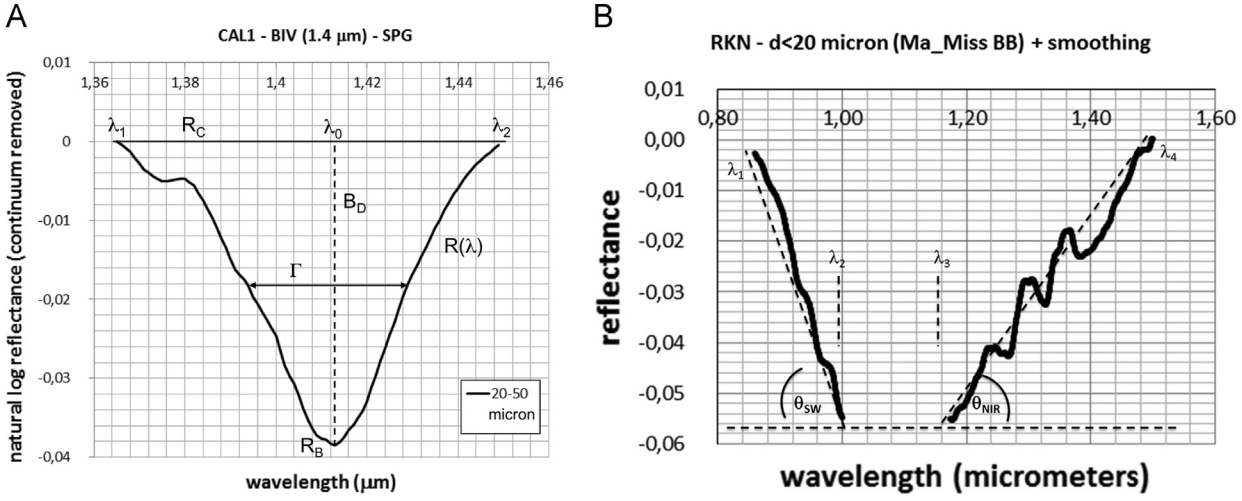

Fig. 5. Determination of band parameters; the spectrum here is showed in natural log reflectance, after continuum removal. (A) For carbonate samples (CAL1 in the example), the band center, depth and area are determined for each considered band. (B) For volcanic samples, because the gap at 1 μm overlaps with the band center, we have determined different parameters: the band area (outside the gap), the band slope on the SW and LW side (angle θ_{SW} and θ_{LW}) and an asymmetry parameter ($p=\theta_{SW}/\theta_{LW}$).

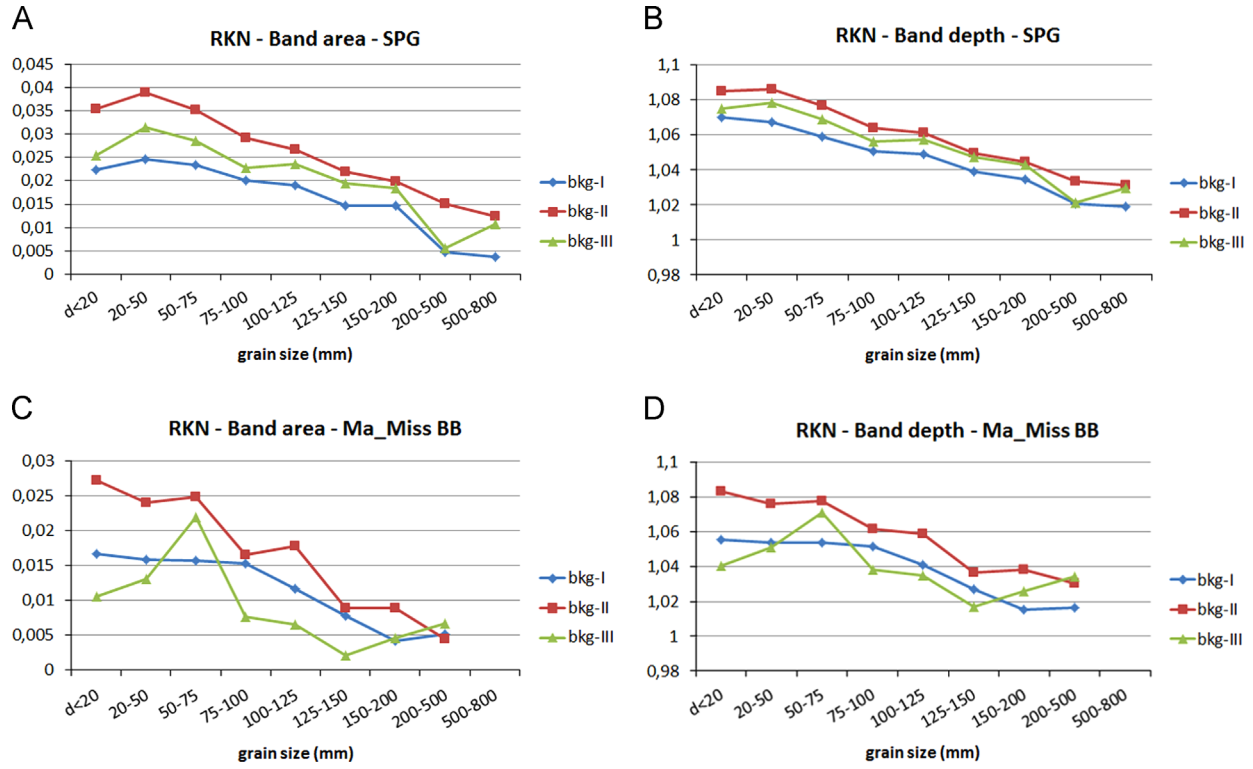

Fig. 6. Sample RKN. A and C: band area at 1 μm computed from SPG and Ma_Miss data, respectively, using three different polynomials as continuum background (straight line (I), parabolic (II) and cubic (III)). B and D: band depth at 1 μm computed from SPG and Ma_Miss data, respectively, using three different polynomials as continuum background.

Table 1
Choice of continuum background, for SPG measurements. Depending on the degree of polynomial chosen for the background removal (straight line, parabolic or cubic) an error is committed.

Choice of continuum background – Error estimate – SPG				
Grain size	Δ – Area% (I vs. II)	Δ – Area% (I vs. III)	Δ – Depth% (I vs. II)	Δ – Depth% (I vs. III)
$d < 20$ μm	57.26	13.48	1.38	0.45
20–50	57.92	28.09	1.79	1.08
50–75	49.83	21.74	1.64	0.93
75–100	46.02	13.36	1.28	0.53
100–125	40.25	24.12	1.15	0.80
125–150	49.94	32.33	1.01	0.78
150–200	35.64	26.18	0.98	0.82
200–500	212.88	17.05	1.24	0.09
500–800	226.68	185.70	1.22	1.02
$<\Delta>$ (%)	**86.27**	**40.23**	**1.30**	**0.72**

Table 2
Choice of continuum background, for Ma_Miss BB measurements. Depending on the degree of polynomial chosen for the background removal (straight line, parabolic or cubic) an error is committed.

Choice of continuum background – Error estimate – Ma_Miss BB				
Grain size	Δ – Area% (I vs. II)	Δ – Area% (I vs. III)	Δ – Depth% (I vs. II)	Δ – Depth% (I vs. III)
$d < 20$ μm	64.23	36.24	2.63	1.45
20–50	51.05	18.24	2.10	0.31
50–75	59.42	40.48	2.25	1.61
75–100	8.58	50.17	0.96	1.31
100–125	51.49	43.98	1.67	0.60
125–150	13.29	73.36	0.95	0.94
150–200	115.29	10.04	2.26	1.05
200–500	15.13	27.26	1.38	1.76
500–800				
$<\Delta>$ (%)	**47.31**	**37.47**	**1.77**	**1.13**

The slopes of the Short and Long Wavelength parts of the band at 1 μm have been plotted vs. the grain size (Fig. 7B and C) and the trend is decreasing as the grain size increases.

The asymmetry parameter (Fig. 7D), for this sample, in function of the grain size decreases as the grain size increases, for SPG, while increases for Ma_Miss BB data.

3.2. San Bartolo Lava/Stromboli (STR72)

The San Bartolo Lava sample shows a unique absorption band near 1 μm (spectra in Figs. 1C and 3C, obtained with SPG and BB, respectively). Band parameters from Ma_Miss spectra have been determined for all grain sizes except the larger one (500–800 μm), where the spectrum was to flat and noisy in the 1-μm region.

Area values (Fig. 8A) from SPG data are also characterized by a decreasing trend towards coarser grains. Area values from BB spectra also show a net decreasing trend, although with some fluctuation, shifted downward of about 30%.

The 1-μm band SW and LW slope show a net decreasing trend vs. grain size, for SPG and Ma_Miss data (Fig. 8B and C).

The asymmetry parameter shows a decreasing trend (Fig. 8D) for SPG and Ma_Miss data.

3.3. Scoria from Vulcanello/Vulcano (VL0)

The spectra of VL0 sample are showed in Figs. 1D and 3D for SPG and BB setup respectively. Spectra show only the Fe^{2+} band near 1 μm; SPG data also show very faint features in the 0.5–0.7 μm region, but here we did not consider them.

Band areas from both SPG and BB data (Fig. 9A) show a decreasing trend with increasing grain size; values from BB spectra are shifted downwards of about 50%.

The 1-μm SW slope shows a net decreasing trend for SPG data (Fig. 9B), while for BB data the trend again seems to be opposite. The 1-μm LW slope seems to be increasing for both instruments (Fig. 9C).

The asymmetry parameter (Fig. 9D) also shows two opposite trends for SPG and Ma_Miss data. The "step" that appears at the 75–100 μm grain size is due to a net change in the trends of SW and LW-slope.

3.4. Scoria of "La Sommata"/Vulcano (VL168/12)

Spectra of sample VL168/12 are depicted in Figs. 1E and 3E. The main absorption band is the one near 1 μm. Other weak features (Fe^{2+} spin forbidden and Fe-metal charge transfer (IVCT)) appear

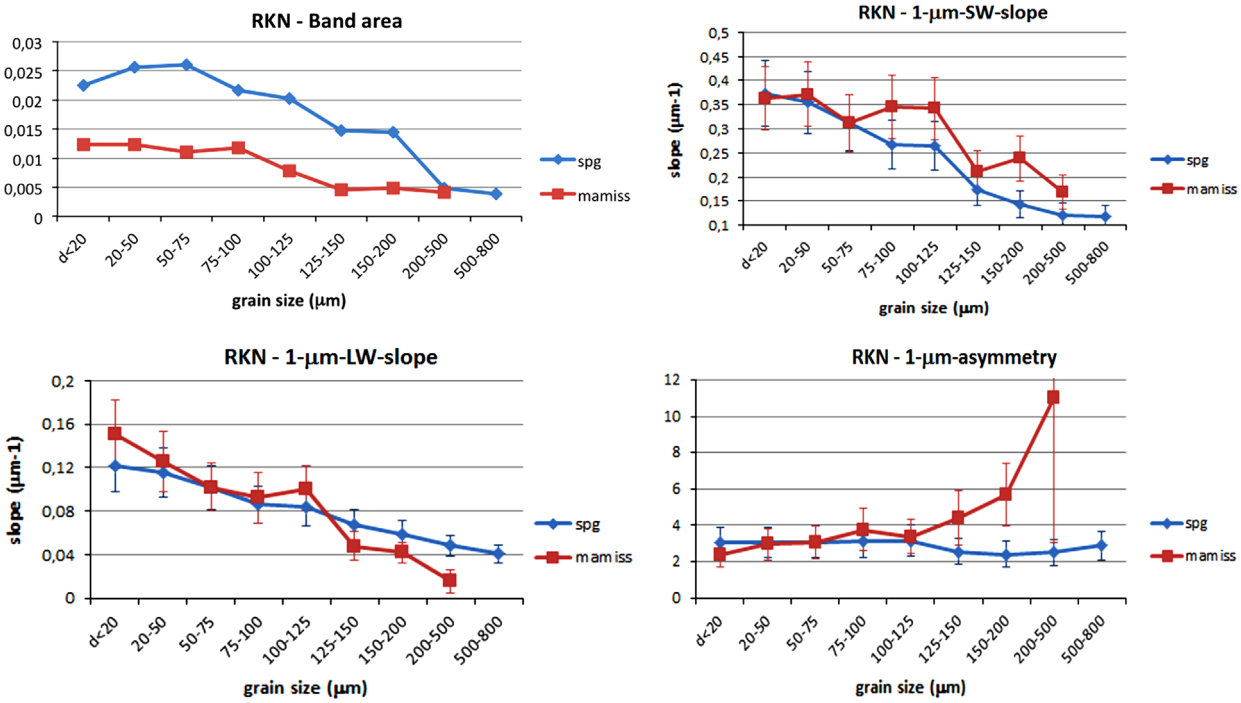

Fig. 7. Spectral parameters relative to the band near 1 μm, for the RKN sample. A: area. B: band SW-slope. D: band LW-slope. C: asymmetry parameter.

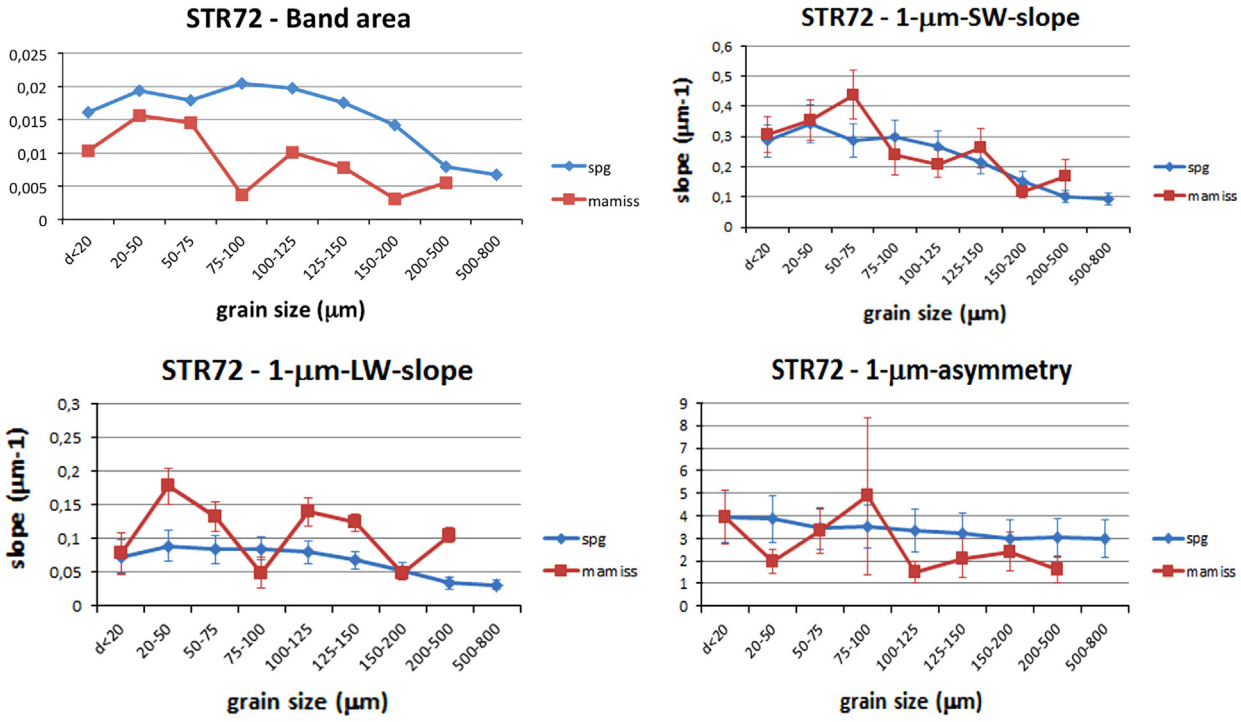

Fig. 8. Spectral parameters relative to the band near 1 μm, for the STR72 lava sample. A: area. B: band SW-slope. C: asymmetry parameter.

in the 0.5–0.9 μm region (e.g. Burns, 1993), but here we neglected them.

Band areas for this sample have been retrieved only for the first five grain size (from <20 μm to 100–125 μm) from Ma_Miss data, because spectra of larger grain sizes were too flat and noisy in the 1-μm region. Band slope and asymmetry have been retrieved for grain sizes from <20 μm to 150–200 μm.

Area values (Fig. 10A) show consistent decreasing trends towards coarser grains, although Ma_Miss BB data are shifted downwards of about 30% on average.

Calculated values of 1-μm band SW and LW slope (Fig. 10B and C) show a net decreasing trend, for increasing grain size. Concerning the asymmetry parameter (Fig. 10D), it is decreasing for SPG data and substantially increasing for Ma_Miss BB data.

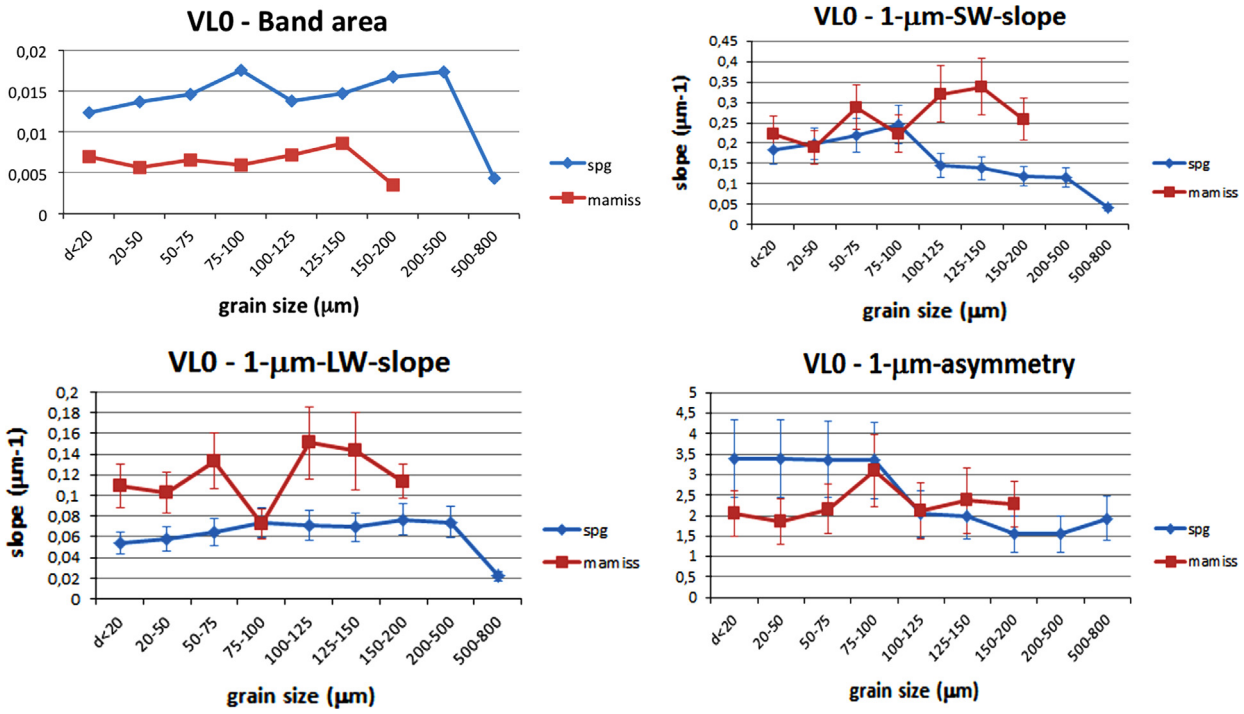

Fig. 9. Spectral parameters relative to the band near 1 μm, for the VL0 sample. A: area. B: band SW-slope. C: asymmetry parameter.

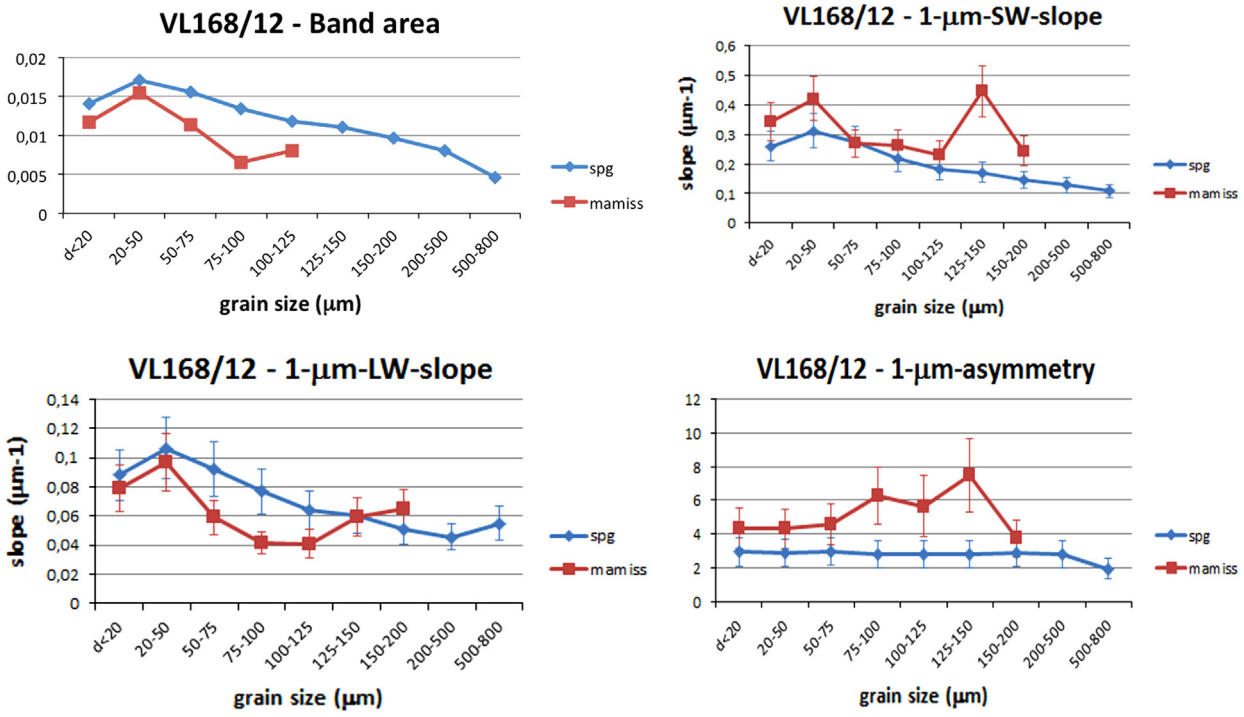

Fig. 10. Spectral parameters relative to the band near 1 μm, for the VL168/12 sample. A: area. B: band Vis-slope.

3.5. Red micritic limestone/Gubbio (CAL1)

The spectra of the micritic limestone sample CAL1 are depicted in Figs. 1B (SPG) and 3B (Ma_Miss BB). They are characterized by evident absorptions at 1.4 μm (OH^-), 1.9 μm (H_2O) and 2.2 μm (CO_3^{2-}; Gaffey (1986), Clark et al. (1990), Clark (1999)); the carbonate band at 2.35 μm is not considered here, because out from the spectral range of Ma_Miss. Very faint features are also visible near 0.75 and 0.9 μm, perhaps due to Fe^{2+}–Fe^{3+} Intervalence Charge Transfer (IVCT, but not considered here).

The band centers of the four considered bands vs. the grain size are showed in Fig. 11. The centers of 1.4 and 1.9 μm absorptions are nearly constant for both setup. The center of 1.4-μm band from SPG data is equal to 1.41 μm, while center values from BB spectra range within 1.40–1.42 μm. Regarding the 1.9 μm band, both values from SPG and BB spectra are at about 1.91 μm.

The absorption in the 2.2 μm region is at about 2.21 μm for all grain sizes for SPG data; concerning Ma_Miss BB spectra, the feature appears at about 2.15–2.16 μm.

Band depths vs. the grain size are depicted in Fig. 12. Depth values at 1.4 μm from SPG data decrease towards coarser grains, except for the grain-size $d < 20$ μm; these values are in the range 1.03–1.04. Depth values of the same band from BB spectra also show a decreasing trend; data from 50–75 to 500–800 μm dimensional class to the nine are in the range 1.07–1.01, while the < 20 and 20–50 μm classes show higher depth values, near 1.7 and 1.3, respectively.

Band depth at 1.9 μm also shows decreasing trends in SPG and BB data. Depth values from SPG are in the range 1.14–1.11; BB data decrease from 1.31 to 1.09 (classes from 50–75 to 500–800 μm), while values for the finest two classes are in the range 2–8.

Regarding the band at 2.2 μm, BB data values have a decreasing trend from 1.71 to 1.05; SPG data also have a decreasing trend, for classes from 20–50 to 500–800 μm but assume smaller values (1.03–1.02).

Band area values vs. grain size are showed in Fig. 13. Concerning the band at 1.4 μm, data from both SPG and BB spectra show decreasing trends, increasing the grain size. SPG values are in the range 0.0014–0.0010, while BB values are in the range 0.002–0.0003 (classes from 50–75 to 500–800 μm). Band depths relative to the first two grain size classes for BB are higher by a factor 10.

Band areas for 1.9-μm feature decrease for both instruments datasets, although values are within a factor of about 2.

Relatively to the 2.2-μm feature both datasets show consistent decreasing trends, but with values within a factor of about 3–10.

3.6. Calcite/Rif.Jorio – Apennines (JOR1)

Calcite sample spectra are shown in Figs. 1A (SPG setup) and 3A (BB setup).

SPG spectra are characterized by absorptions near 1.5 μm (OH) and 1.9 μm (H_2O), and by features at 1.75, 2.2 and 2.35 μm (CO_3; Gaffey (1986), Clark et al. (1990), Clark (1999)). Spectra also show a drop off of reflectance short-ward of about 1 μm, that increases with coarser grains.

Ma_Miss BB spectra are characterized by weaker absorptions: the 1.5-μm feature, the band at 1.9 μm (clearly visible in spectra of intermediate grains), and the carbonate bands at 2.2 μm. The other carbonate feature near 1.75 μm is not discernible in BB spectra.

Here we considered the common features, thus neglecting the one at 1.75 μm; moreover we neglected the carbonate band at 2.35 μm, visible only in SPG spectra.

The band centers are showed in Fig. 14 vs. the grain size. Regarding the 1.4-μm band the centers are in the range 1.46–1.47 μm (SPG data) and 1.43–1.46 μm (BB data) for most classes except the finest, where the OH^- band appears to be centered at 1.54 μm. Concerning the H_2O band, the centers are in the range 1.94–1.95 μm (SPG spectra) and 1.86–1.98 μm (BB spectra). The considered carbonate band is centered at 2.16 μm in SPG spectra, while in BB spectra the position varies in the range 2.15–2.18 μm.

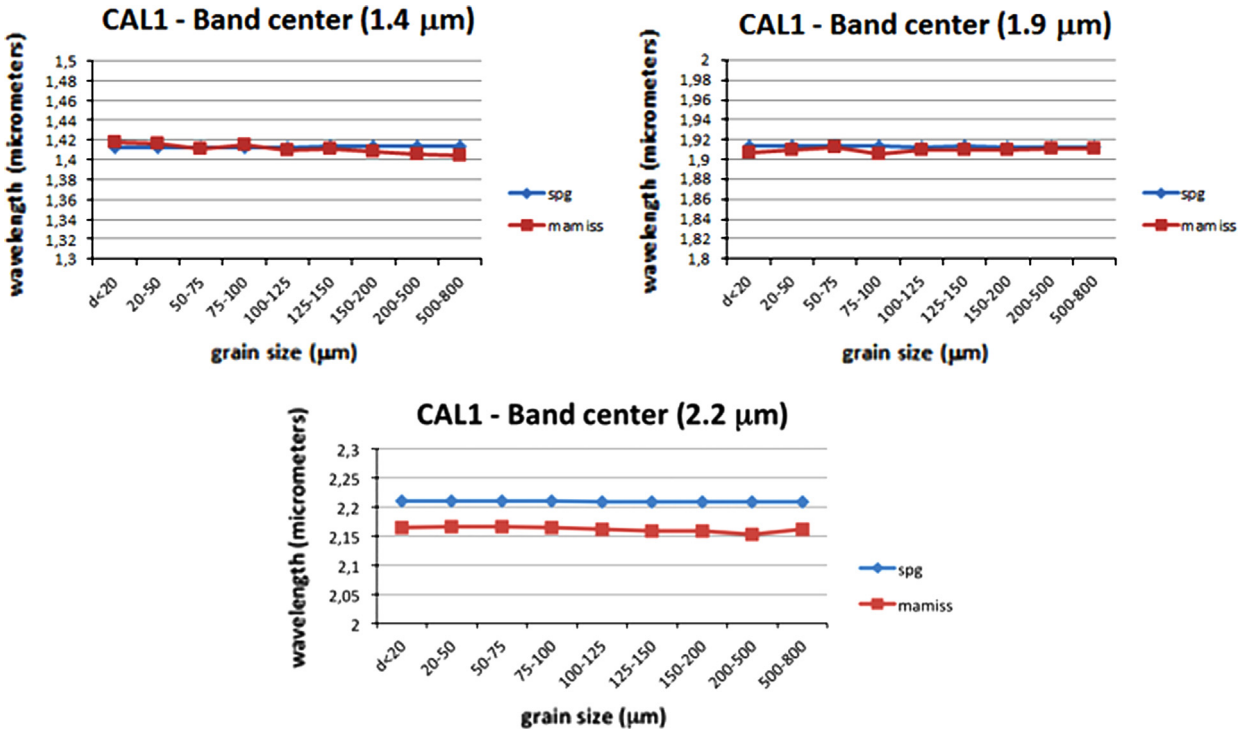

Fig. 11. Sample CAL1. Band center of absorptions at 1.4 μm (A), 1.9 μm (B), and 2.2 μm (C).

The band depths are showed in Fig. 15. The 1.4, 1.9 and 2.2-μm features show different trends with respect to other samples. The band depth (SPG spectra) increases as the grain size increases, reaching a maximum for the dimensional class 125–150 μm and then decreasing towards coarser grains. Band depths from BB spectra instead show an almost opposite trend, with a minimum corresponding to the dimensional class 125–150 μm.

Area values vs. the grain size are depicted in Fig. 16. The resulting trends appear to be similar to those for band depths. Values from SPG spectra relative to 1.4, 1.9 and 2.2-μm bands increase for increasing grain size, with a maximum corresponding to the class 125–150 μm (as for band depths), and then decrease for larger grains. Area values from BB spectra are characterized by an opposite trend, having a minimum corresponding to the same dimensional class.

4. Discussion

The analyzed spectral parameters follow trends that are mostly consistent between the two instruments, although few discrepancies are present. Two different set of parameters have been

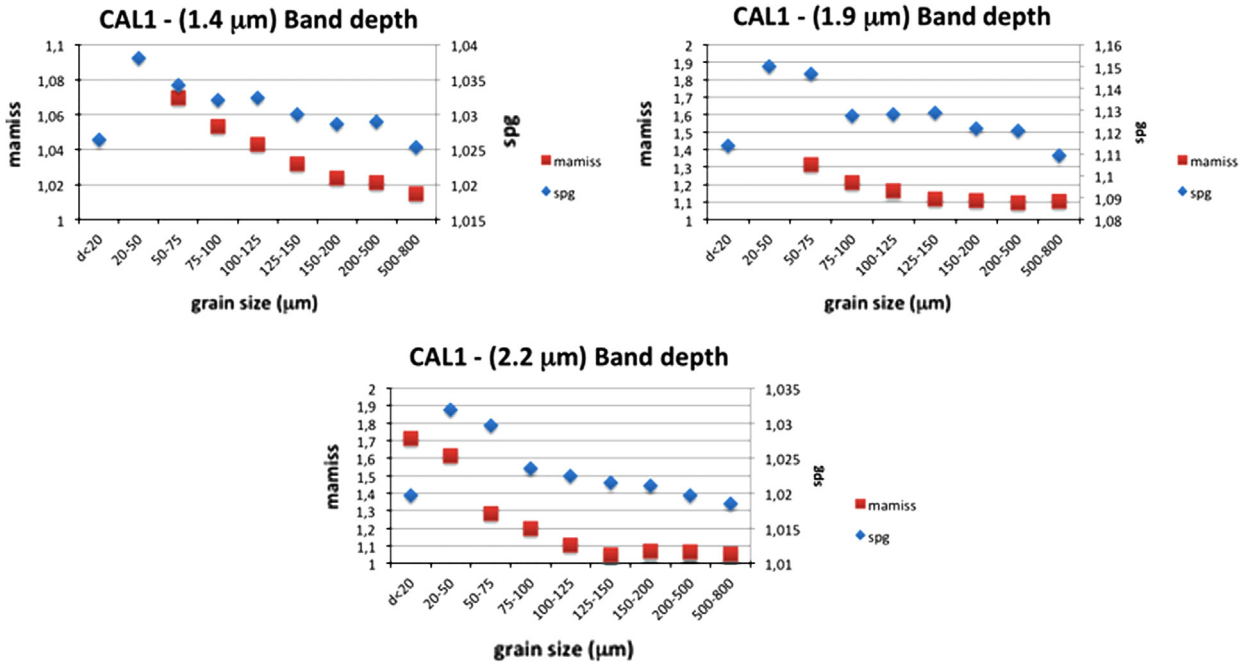

Fig. 12. Sample CAL1. Band depth of absorptions at 1.4 μm (A), 1.9 μm (B), and 2.2 μm (C).

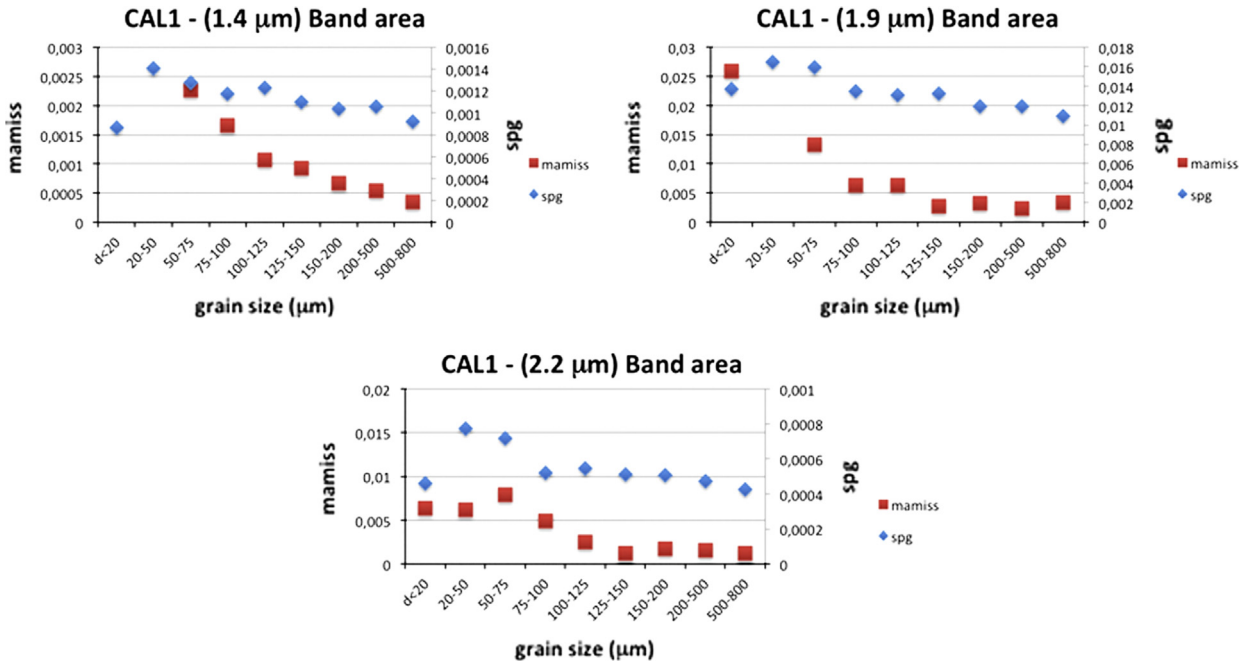

Fig. 13. Sample CAL1. Band area of absorptions at 1.4 μm (A), 1.9 μm (B), 2.2 μm (C).

analyzed for carbonates and volcanics., For the former band center, depth and area of the features at 1.4, 1.9 and 2.2 μm have been derived, while for the latter the following parameters have been used to investigate the 1.0 μm absorption bands: the band area, the slope of the Vis side of the band, and the asymmetry parameter. Ma_Miss breadboard spectra are characterized by a gap of some tens of nanometers at the wavelengths of 1.0 and 1.8 μm, thus causing uncertainty in the band center and depth at 1.0 μm. For this reason, these two parameters at 1.0 μm have not been derived for the volcanic samples.

Concerning a generic band parameter *B*, in order to estimate the fluctuation with respect to the mean, for each band and for the

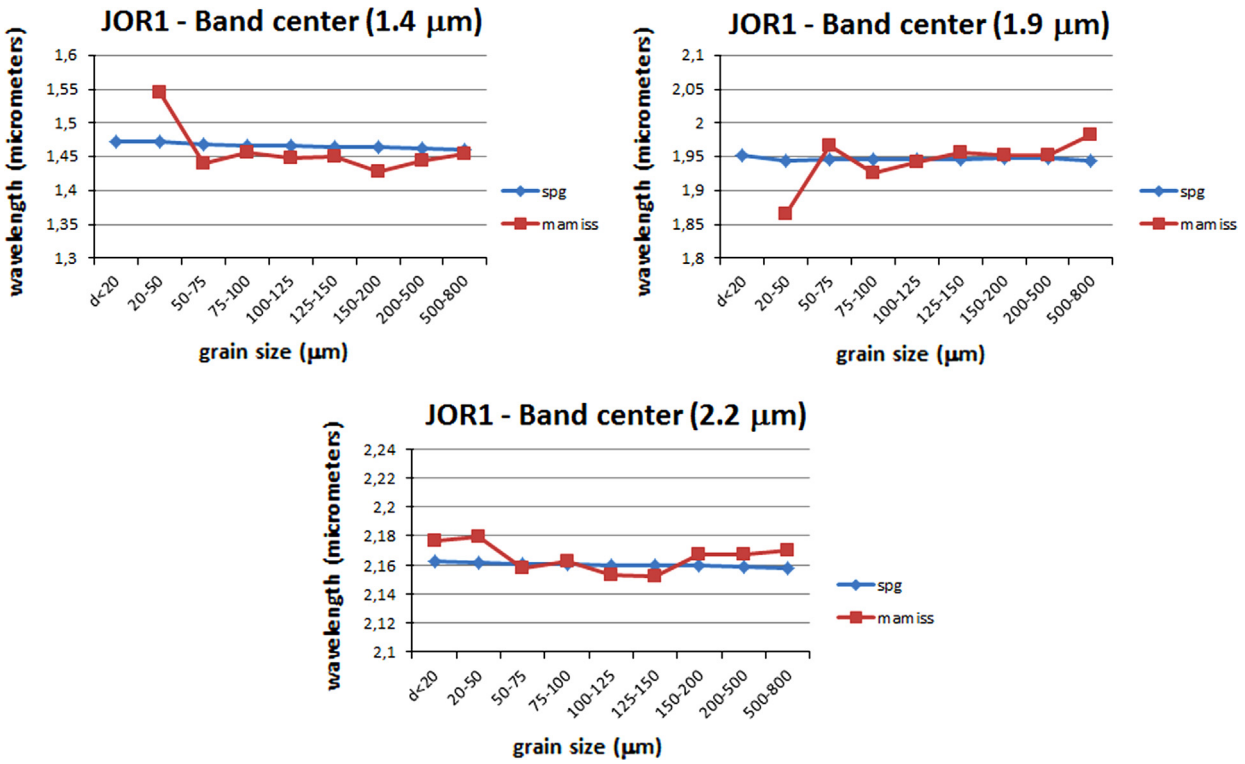

Fig. 14. Sample JOR1. Band center of absorptions at 1.4 μm (A), 1.9 μm (B), and 2.2 μm (C).

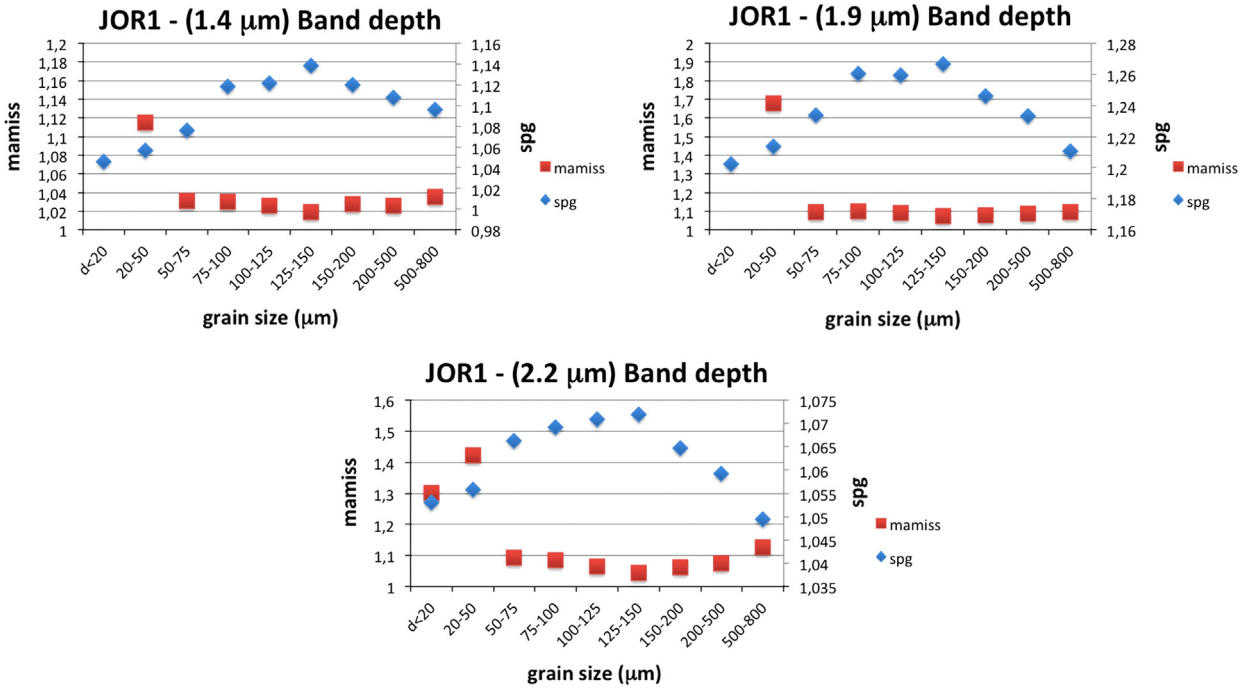

Fig. 15. Sample JOR1. Band depth of absorptions at 1.4 μm (A), 1.9 μm (B), and 2.2 μm (C).

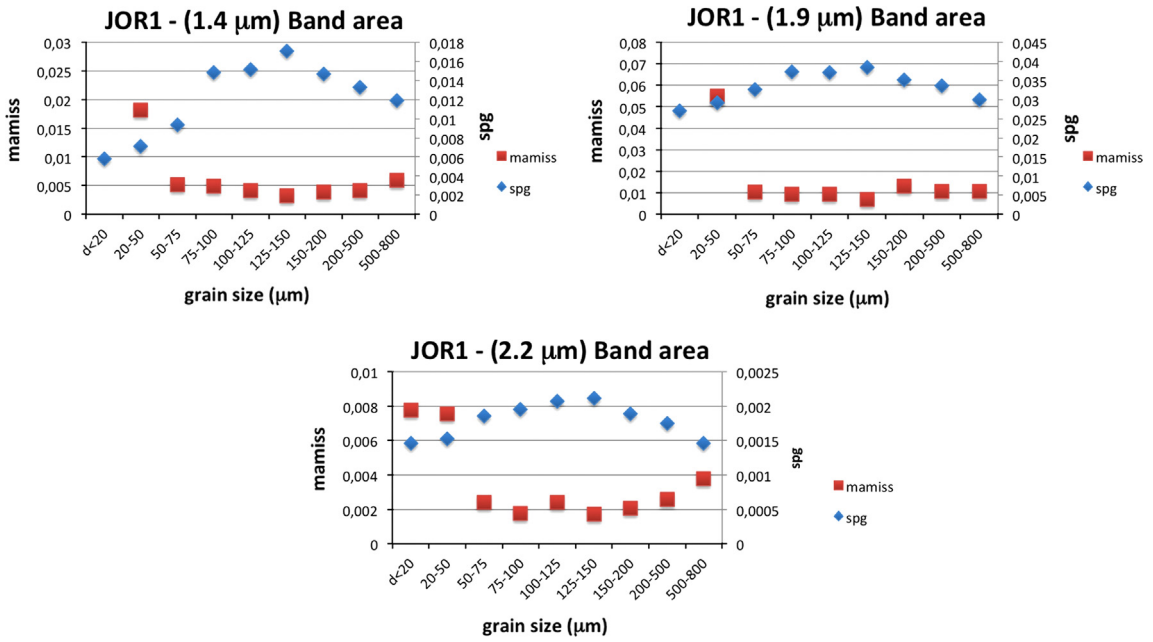

Fig. 16. Sample JOR1. Band area of absorptions at 1.4 μm (A), 1.9 μm (B), and 2.2 μm (C).

*i*th grain size of the various samples the relative percent variation has been calculated as follows:

$$\Delta B(\%) = \frac{|B(ith\ grain\ size) - \bar{B}|}{\bar{B}} \times 100$$

where $\bar{B}$ has been averaged on all the grain sizes of the given sample. The B relative percent variation has been calculated for the spectra acquired by both the instruments.

Subsequently the band parameters obtained from the two instruments have been compared, taking the SPG data as reference. Thus for the *i*th grain size and for each band, the percent variation between the two instruments has been evaluated as follows:

$$\Delta B_{-instr}(\%) = \left| \frac{B(bb) - B(spg)}{B(spg)} \right|_{ith\ grain\ size} \times 100$$

The mean percent variation $\Delta B(\%)$ (for band centers) has been computed averaging on all the dimensional classes. In the following we discuss the comparison results for each class of sample used in this study.

4.1. Volcanics

For volcanic samples the differences between area values ($\Delta B_{A\text{-}instr}(\%)$) are in the range 9–80% (Table 7). Area values obtained from SPG spectra are systematically larger than those obtained from BB spectra: this can be explained by taking into account the fact that BB spectra have the gap at 1.0 μm, and so this fraction must be subtracted by the band area (see Section 3 and Fig. 5B).

The instrumental differences between values of the slope on the Short and Long Wavelength (SW and LW respectively) side of the 1-μm band (θ_{SW} and θ_{LW}, Fig. 5B and Table 8) are mostly in the range 1–40% ($\Delta B_{SW\text{-}instr}(\%)$ and $\Delta B_{LW\text{-}instr}(\%)$), although some values differ by a factor 2. The decreasing in the values of the 1-μm SW and LW-slope, is consistent with the flattening of the spectra towards greater grains sizes. Spectral parameters for the 1-μm feature have been retrieved for all grain sizes from SPG data, while concerning Ma_Miss data, they have not been determined for some larger grain sizes. This is because Ma_Miss spectra of coarser grains are too flat and noisy in that region.

Table 3
Mean centers, fluctuations (respect to average) and mean fluctuation (SPG).

Spectro-Goniometer – band center fluctuations						
	CAL1			JOR1		
	2.2 μm	1.9 μm	1.4 μm	2.2 μm	1.9 μm	1.4 μm
$<B_C>$ (μm)	2.21	1.91	1.41	2.16	1.95	1.47
ΔB_C %						
$d<20$ μm	0.02	0.06	0.06	0.11	0.23	0.48
20–50	0.02	0.03	0.02	0.06	0.09	0.42
50–75	0.02	0.00	0.03	0.03	0.07	0.12
75–100	0.03	0.00	0.02	0.02	0.06	0.00
100–125	0.01	0.01	0.00	0.02	0.08	0.04
125–150	0.01	0.01	0.03	0.02	0.05	0.17
150–200	0.02	0.02	0.02	0.02	0.11	0.13
200–500	0.01	0.03	0.03	0.05	0.10	0.33
500–800	0.05	0.02	0.04	0.11	0.10	0.42
$<\Delta B_C>$ %	0.02	0.02	0.03	0.05	0.10	0.23

The differences between values of asymmetry parameter for the two datasets (Table 9, $\Delta B_{ASYM\text{-}instr}(\%)$) are mostly in the range 0–40%, with a very few cases in which values differ by a factor 1–1.5.

The asymmetry parameter determined from SPG data show a decreasing behavior with increasing grain size, for all the volcanic samples (Figs. 6–9). That is, the 1-μm band SW-slope tends to decrease more slowly than the LW-slope.

The asymmetry parameter computed from Ma_Miss data shows a consistent behavior only for STR72 sample, while the trend is opposite (increasing values towards coarser grains) for RKN, VL0 and VL168/12.

The differences observed between these trends (for SPG and BB data) could be attributed to the different behavior of the spectra. Spectra of RKN sample are characterized by a quicker flattening of the NIR part with respect to the VIS part, for both instruments

(Figs. 1F and 3F). Regarding spectra of STR72 and VL0 measured with Ma_Miss BB setup (Fig. 3C and D), the VIS part tends to be nearly flat for most of the grain sizes.

4.2. Carbonates

The band centers derived from both instrument spectra for carbonate samples (CAL1 and JOR1), are not characterized by any definite correlation with the powder grain size, as expected. Nevertheless the centers obtained from SPG spectra show less variation than the centers derived from BB spectra (see Tables 3 and 4).

Regarding the SPG spectra, the values of $\Delta B_C(\%)$ among the various samples are $<1.5\%$ (Table 3); for BB spectra, the values are $<4\%$ (Table 4).

The displacement of Ma_Miss band centers with respect to SPG centers (see Table 5) is greater for the calcite sample, than for the limestone. Regarding the CAL1 sample the differences in band centers are $<1\%$ for features at 1.4 and 1.9 μm, while are $<2\%$ for the absorption at 2.2 μm. If we consider the JOR1 sample, the displacements are $<2\%$ for all absorption features and all grain sizes except the second (20–50 μm), where the differences are $<5\%$.

In order to estimate the relative displacement between the other parameters from the two instruments (i.e. band depths and areas), the same evaluation has been done as for the band centers. The relative percent variations are listed in Tables 6 and 7 for depths and areas, respectively.

Table 4
Mean centers, fluctuations (respect to average) and mean fluctuation (BB).

Ma_Miss – band center fluctuation						
	CAL1			JOR1		
	2.2 μm	1.9 μm	1.4 μm	2.2 μm	1.9 μm	1.4 μm
$<B_C>$ (μm)	2.16	1.91	1.41	2.17	1.94	1.46
ΔB_C %						
$d<20$ μm	0.17	0.15	0.44	0.54		
20–50	0.18	0.01	0.35	0.65	4.03	5.91
50–75	0.17	0.12	0.00	0.33	1.22	1.19
75–100	0.13	0.20	0.32	0.11	0.90	0.15
100–125	0.02	0.00	0.12	0.57	0.01	0.70
125–150	0.11	0.03	0.03	0.61	0.73	0.53
150–200	0.12	0.05	0.23	0.09	0.49	2.13
200–500	0.41	0.08	0.35	0.10	0.45	0.97
500–800	0.02	0.09	0.44	0.24	2.05	0.24
$<\Delta B_C>$ %						
	0.15	0.08	0.26	0.36	1.24	1.48

Regarding the sample CAL1, the differences in depth values are in the range 0–30% for all dimensional classes above the third (50–75 μm), while greater differences are found for values of the first two classes, differing by a factor 1.5–7. Considering the sample JOR1 the depth values differences between BB and SPG data are in the range 0–40% for all grain sizes.

Band area values show the greatest discrepancies between the two datasets (Table 7). Band area values for CAL1 sample differ by about one order of magnitude at maximum (a factor 10–30), while area values for JOR1 sample differ by about a factor 5 at maximum.

Band depth and area values show differences for carbonate samples: in BB spectra the bands in the range of 1.4–2.2 μm are immersed in noisy data and weaker (smaller spectral contrast) than the corresponding features in SPG spectra (Tables 7–9).

The discrepancy in the behavior of band depths and areas with grains size, concerning calcite (JOR1) spectra (Figs. 15–16), has to be put in relation with the different optical properties that characterize this sample (very optically thin) with respect to the other five samples (optically thick). Same inconsistent trends have been obtained for this sample also analyzing the spectral slope in the VIS range, as discussed in De Angelis et al. (2014).

5. Conclusions

The Ma_Miss miniaturized spectrometer, which will be entirely hosted within the Drill of the ExoMars-2018 Pasteur Rover, will investigate and characterize the mineralogy and stratigraphy of the shallow Martian subsurface. Currently we are evaluating and characterizing the scientific performances of the Ma_Miss laboratory model (the breadboard).

Table 6
Relative percent variations of band depths from Ma_Miss BreadBoard spectra, computed with respect to SPG data.

Ma_Miss vs. Spectro-Goniometer – band depth						
	CAL1			JOR1		
	2.2 μm	1.9 μm	1.4 μm	2.2 μm	1.9 μm	1.4 μm
$\Delta B_{D\text{-}instr}$ %						
$d<20$ μm	68.07	102.37	60.36	23.60		
20–50	56.49	637.06	28.14	34.71	38.14	5.53
50–75	24.70	14.59	3.40	2.50	11.40	4.14
75–100	17.04	7.24	2.05	1.54	12.93	7.86
100–125	7.95	2.97	1.05	0.58	13.31	8.52
125–150	2.71	1.25	0.18	2.56	15.40	10.45
150–200	4.79	1.11	0.50	0.17	13.53	8.19
200–500	4.32	2.30	0.75	1.48	11.97	7.40
500–800	3.23	0.36	1.03	7.36	9.61	5.55

Table 5
Relative percent variations of band centers from Ma_Miss BreadBoard spectra, computed with respect to SPG data.

Ma_Miss vs. Spectro-Goniometer – band center								
	CAL1 – 2.34 μm	CAL1 – 2.2 μm	CAL1 – 1.9 μm	CAL1 – 1.4 μm	JOR1 – 2.34 μm	JOR1 – 2.2 μm	JOR1 – 1.9 μm	JOR1 – 1.4 μm
$\Delta B_{C\text{-}instr}$ %								
$d<20$ μm	0.88	2.01	0.41	0.36	0.12	0.65		
20–50	0.58	1.99	0.23	0.24	0.14	0.82	4.13	4.90
50–75	0.61	2.00	0.07	0.11	0.04	0.13	1.09	1.84
75–100	0.96	2.06	0.40	0.21	0.02	0.10	1.04	0.69
100–125	0.86	2.12	0.19	0.26	0.10	0.33	0.13	1.27
125–150	0.72	2.25	0.18	0.14	0.09	0.36	0.59	0.89
150–200	0.62	2.25	0.13	0.40	0.03	0.34	0.18	2.53
200–500	0.42	2.54	0.09	0.52	0.02	0.37	0.15	1.17
500–800	0.52	2.12	0.09	0.62	0.06	0.58	1.96	0.36

Table 7
Relative percent variations of band areas from Ma_Miss BreadBoard spectra, computed with respect to SPG data.

Ma_Miss vs. Spectro-Goniometer – band area										
	RKN	STR72	VL0	VL168/12	CAL1 – 2.2 μm	CAL1 – 1.9 μm	CAL1 – 1.4 μm	JOR1 – 2.2 μm	JOR1 – 1.9 μm	JOR1 – 1.4 μm
$\Delta B_{A\text{-}instr}$ %										
$d < 20$ μm	26.16	30.19	43.15	16.56	1290.00	89.59	3149.48	428.94		
20–50	32.60	19.15	58.64	9.33	704.80	629.70	671.66	393.39	88.06	155.01
50–75	33.50	19.63	55.11	27.03	1005.42	16.80	77.54	29.00	68.26	44.19
75–100	24.23	77.97	67.10	55.50	841.73	52.63	41.28	10.26	74.71	66.98
100–125	38.49	20.20	48.84	36.50	355.39	51.53	12.68	16.17	74.51	72.32
125–150	47.12	53.49	41.52	42.19	134.96	79.11	15.36	18.90	82.43	81.29
150–200	71.57	73.95	80.57	58.36	234.85	73.25	35.77	9.58	62.85	73.43
200–500	7.49	15.56			222.03	80.86	48.67	47.63	68.02	69.09
500–800					177.28	69.30	62.23	157.65	64.23	50.28

Table 8
Relative percent variations of 1-μm band SW- and LW-slope from Ma_Miss BreadBoard spectra computed with respect to SPG data.

Ma_Miss vs. Spectro-Goniometer								
1-μm *band short wavelength-slope*					1-μm *band long wavelength-slope*			
	RKN	STR72	VL0	VL168/12	RKN	STR72	VL0	VL168/12
$\Delta B_{SW\text{-}instr}$ %					$\Delta B_{LW\text{-}instr}$ %			
$d < 20$ μm	2.40	7.07	21.80	32.24	24.26	5.90	102.55	10.29
20–50	2.61	3.02	4.11	34.86	8.63	99.08	75.62	8.87
50–75	0.24	53.14	31.93	1.07	1.12	57.71	105.96	36.06
75–100	29.04	19.55	9.27	20.29	7.01	42.03	1.97	45.88
100–125	29.02	22.02	120.46	27.11	20.41	74.03	111.78	36.46
125–150	21.78	20.39	145.14	159.45	29.03	82.07	105.60	2.32
150–200	66.99	22.92	116.97	67.17	29.11	4.67	48.61	28.01
200–500	39.17	66.23			68.14	213.67		
500–800								

Spectroscopic measurements have been performed on six samples, four volcanic rocks and two carbonates (in powder form and sieved into nine different grain sizes) using two distinct experimental setup: (a) the Ma_Miss breadboard (BB), (b) the Spectro-goniometer setup (SPG), both in use in the laboratory at INAF – IAPS.

While in a previous paper (De Angelis et al., 2014) we have analyzed the continuum slope and the reflectance level, here we focused our discussion on the band parameters.

Regarding the two carbonate samples, we investigated the absorptions at 1.4, 1.9 and 2.2 μm. In these cases, the Band Center, Depth and Area have been determined.

Band centers are mutually consistent within few percent. Depth and area values, obtained from the two datasets, show consistent trends vs. grain size (decreasing towards coarser grains) for the limestone sample (CAL1), while they show opposite trends for the calcite (JOR1). These differences can be attributed mainly to different optical properties that characterize the two samples.

For what concerns the volcanic samples, the absorption feature at 1 μm has been analyzed, that is the only detectable absorption band, except the water feature appearing in one sample. Because BB spectra show a gap in the data at 1.0 and 1.8 μm, corresponding to the junctions between the detectors, we have not determined the center and depth of the 1-μm band. Thus, for this absorption we derived the following parameters:

1-μm band slope on the Short Wavelength side and Long Wavelength side

Band asymmetry

Band area corrected for the gap

Area values determined with the two setups show trend that are mutually consistent: there is a net decrease with increasing grain size. The SW slope of the 1-μm band shows a decreasing trend with increasing grain size (spectra become more flattened), for all SPG data; this parameter also shows a net decreasing trend for all Ma_Miss spectra, except VL0. The LW-slope of the 1-μm band (SPG data) has a decreasing behavior for RKN, STR72 and VL168/12 and an increasing trend for VL0 sample. The LW-slope (Ma_Miss BB data) also has a net decrease for what concerns RKN, STR72 and VL168/12 samples, while for VL0 the trend is ambiguous.

Table 9
Relative percent variations of 1-μm band asymmetry from Ma_Miss BreadBoard spectra computed with respect to SPG data.

Ma_Miss vs. Spectro-Goniometer – 1-μm *band asymmetry*				
	RKN	STR72	VL0	VL168/12
$\Delta B_{ASYM\text{-}instr}$ %				
$d < 20$ μm	21.45	1.10	39.87	47.42
20–50	21.43	48.25	45.40	47.98
50–75	1.35	2.90	35.95	54.73
75–100	20.59	38.76	7.45	122.27
100–125	7.15	55.19	4.10	100.05
125–150	71.60	33.88	19.23	165.61
150–200	135.57	19.15	46.00	30.59
200–500	336.83	47.01		
500–800				

The asymmetry parameter always shows a net decreasing trend for SPG data, while for Ma_Miss data the trend is decreasing only for STR72 sample. This apparent discrepancy is probably due to the different behavior of the VIS and NIR parts (and thus to their ratio) of the spectra of the samples, as seen by the two instruments. Nevertheless substantially the trend of SW-slope and LW-slope as seen by the two instruments are almost always consistent.

The differences seen between the two instruments, due to differences in the viewing geometries and in general between the

two experimental setups, cause some spectral parameters (band slopes, areas) to have different absolute values, while others (i.e. reflectance continuum) show similar absolute values. Nevertheless the observed trends (spectral parameters vs. the grain size) are generally consistent with each other, even if discrepancies arise in some cases. This does not affect severely the interpretation of Ma_Miss data: Ma_Miss breadboard proves to have capabilities suitable to provide useful spectroscopic information, and so to investigate composition and mineralogy of different materials. The diagnostic absorption bands of different minerals are clearly visible within the operative spectral range; the albedo (reflectance) and grain size information can be retrieved from Ma_Miss trends for most of samples. Other analyzed parameters (i.e. band depth, area and slope) are also related to grain size, and can in principle help in retrieving relative abundances in mineral mixtures: this aspect will be the subject of future work.

Acknowledgments

We wish to thanks the Italian Space Agency (ASI) for funding and fully supporting the Ma_Miss experiment (ASI/INAF grant I/060/10/0). We also thank G.F. De Astis (INGV) for providing the Aeolian samples, and A.Frigeri for providing the red micritic limestone. We thank an anonymous reviewer for useful comments and suggestions.

Appendix A. Supplementary information

Supplementary data associated with this article can be found in the online version at doi:10.1016/j.pss.2015.07.002.

References

Baker, V.R., 2001. Water and the martian landscape. Nature 412 (12), 228–236.
Bandfield, J.L., et al., 2000. A global view of martian surface compositions from MGS-TES. Science 287, 1626. http://dx.doi.org/10.1126/science.287.5458.1626.
Bandfield, J.L., 2002. Global mineral distributions on Mars. J. Geophys. Res. 107 (E6), 5042. http://dx.doi.org/10.1029/2001JE001510.
Bibring, J.-P., 2005. Comparative planetology, Mars and exobiology. In: Gargaud, Muriel, Barbier, Bernard, Martin, Hervé, Reisse, Jacques (Eds.), Lectures in Astrobiology, I. Springer, Berlin, cap.9.
Boynton, W.V., et al., 2002. Distribution of Hydrogen in the near surface of Mars: evidence for subsurface ice deposits. Science 297, 81. http://dx.doi.org/10.1126/science.1073722.
Boynton, W.V., et al., 2009. Evidence for calcium carbonate at the Mars Phoenix landing site. Science 325, 61. http://dx.doi.org/10.1126/science.1172768.
Burns, R.G., 1993. Mineralogical Applications of Crystal Field Theory. Cambridge University Press, United Kingdom, p. 551.
Carr, M.H., Schaber, G.G., 1977. Martian permafrost features. J. Geophys. Res. 8 (28), 4039–4054.
Carr, M.H., Head III, J.W., 2003. Oceans on Mars: an assessment of the observational evidence and possible fate. J. Geophys. Res. 108 (E5), 5042. http://dx.doi.org/10.1029/2002JE001963.
Carr, M.H., Head III, J.W., 2010. Geological history of Mars. Earth Planet. Sci. Lett. 294, 185–203.
Christensen, P.R., et al., 2005. Evidence for magmatic evolution and diversity on Mars from infrared observations. Nature 436, 504–509. http://dx.doi.org/10.1038/nature03639.
Clark, R.N., Roush, T.L., 1984. Reflectance spectroscopy: quantitative analysis techniques for remote sensing applications. J. Geophys. Res. 89 (B7), 6329–6340.
Clark, R.N., et al., 1990. High spectral resolution reflectance spectroscopy of minerals. J. Geophys. Res. 95 (B8), 12,653–12,680.
Clark, R.N., 1999. Chapter 1: Spectroscopy of rocks and minerals, and principles of spectroscopy. In: Rencz, A.N. (Ed.), Manual of Remote Sensing, Vol. 3. John Wiley and Sons, New York, pp. 3–58.
Coradini, A., et al., 2001. MA_MISS: Mars Multispectral Imager for Subsurface Studies. Adv. Space Res. 28 (8), 1203–1208.
Coradini, A., et al., 2005. MILLBILLILLIE: Reflectance spectroscopy, Asteroid, Comets, Meteors – IAU Symposium 229, Rio de Janeiro, 7-12-2005.
De Angelis, S., et al., 2014. The Ma_Miss instrument performance, I: analysis of rocks powders by Martian VNIR spectrometer. Planet. Space Sci. 101, 89–107 http://dx.doi.org/10.1016/j.pss.2014.06.010.
Di Achille, G., et al., 2013. High resolution morphometry and mineralogy of the shalbatana paleo-lacustrine deposits (Mars) using MRO HiRISE and CRISM Data. In: Proceedings of the 44th Lunar and Planetary Science Conference. Abstract no. 3027.
Dohm, J.M., et al., 2009. GRS evidence and the possibility of paleooceans on Mars. Planet. Space Sci. 57, 664–684.
Edgett, K.S., et al, 2013. Curiosity's Mars Hand Lens Imager (MAHLI): Sol 0–179 activities, observations, range and scale characterization, EPSC Abstracts Vol. 8, EPSC2013-246, European Planetary Science Congress (London).
Ehlmann, B.L., et al., 2008. Orbital identification of Carbonate-Bearing Rocks on Mars. Science 322, 1828–1832.
Ehlmann, B.L., Edwards, C.S., 2014. Mineralogy of the Martian Surface. Annu. Rev. Earth Planet. Sci. 42, 291–315.
Gaffey, S., 1986. Spectral reflectance of carbonate minerals in the visible and near infrared (0.35–2.55 μm): calcite, aragonite and dolomite. Am. Mineral. 71, 151–162.
Gendrin, A., et al., 2005. Sulfates in Martian layered terrains: the OMEGA/Mars Express view. Science 307, 1587.
Grotzinger, J.P., et al., 2012. Mars science laboratory mission and science investigation. Space Sci. Rev. 170, 5–56. http://dx.doi.org/10.1007/s11214-012-9892-2.
Gupta, S., et al., 2013. Cross-stratified sedimentary rocks observed by the Mars Science Laboratory Sol 0-180-evidence for fluvial sedimentary transport, EPSC Abstracts Vol. 8, EPSC2013-781-1, European Planetary Science Congress (London).
McEwen, A.S., et al., 2013. Recurring slope lineae in equatorial regions of Mars. Nat. Geosci. 7, 53–58. http://dx.doi.org/10.1038/NGEO2014.
McSween Jr, H.Y., et al., 2009. Elemental composition of the martian crust. Science 324, 736. http://dx.doi.org/10.1126/science.1165871.
Murchie, S.L., et al., 2009. A synthesis of Martian aqueous mineralogy after 1 Mars year of observations from the Mars Reconnaissance Orbiter. J. Geophys. Res. 114 (E00D06). http://dx.doi.org/10.1029/2009JE003342.
Mustard, J.F., et al., 1997. In situ compositions of Martian volcanics: implications for the mantle. J. Geophys. Res. 102 (E11), 25,605–25,615.
Nachon, M., et al., 2013. Sulfate calcium veins observed by the ChemCam instrument onboard Curiosity. European Planetary Science Congress. London, EPSC Abstracts, vol. 8, EPSC2013-534.
Niles, P.B., et al., 2013. Geochemistry of carbonates on Mars: implications for climate history and nature of aqueous environments. Space Sci. Rev. 174, 301–328. http://dx.doi.org/10.1007/s11214-012-9940-y.
Palomba, E., 2009. Evidence for Mg-rich carbonates on Mars from a 3.9 μm absorption feature. Icarus 203, 58–65.
Poulet, F., et al., 2005. Phyllosilicates on Mars and implications for early martian climate. Nature 438, 623–627. http://dx.doi.org/10.1038/nature04274.
Rice, M.S., et al., 2013. Mastcam multispectral imaging results from the Mars Science Laboratory investigation in Yellowknife Bay. 2013 European Planetary Science Congress. London, EPSC Abstracts, vol. 8, EPSC2013-762.
Squyres, S.W., et al., 2004. In situ evidence for an ancient aqueous environment at Meridiani Planum, Mars. Science 306, 1709–1714. http://dx.doi.org/10.1126/science.1104559.
Vago, J.L., et al., 2013. ExoMars, ESA's next step in Mars exploration. ESA Bull. Mag. 155, 12–23.
Williams, R.M.E., et al., 2013. Martian fluvial conglomerates at gale crater. Science 340, 1068. http://dx.doi.org/10.1126/science.1237317.
Wray, J.J., et al., 2011. Evidence for regional deeply buried carbonate-bearing rocks on Mars. In: Proceedings of the 42nd Lunar and Planetary Science Conference. Abstract no. 2635.
Wray, J.J., et al., 2013. Infrared spectral identification of unusually feldspar-rich rocks on Mars. In: Proceedings of the 44th Lunar and Planetary Science Conference. Abstract no. 3065.